Engineering Fracture Mechanics 110 (2013) 421–429

Contents lists available at SciVerse ScienceDirect

Engineering Fracture Mechanics

journal homepage: www.elsevier.com/locate/engfracmech

The effect of the embrittlement on the fatigue limit and crack propagation in a duplex stainless steel during high cycle fatigue

M.C. Marinelli [a,b,*], U. Krupp [b], M. Kübbeler [c], S. Hereñú [a], I. Alvarez-Armas [a]

[a] Instituto de Física Rosario – CONICET, Universidad Nacional de Rosario, Argentina
[b] Faculty of Engineering and Computer Science, University of Applied Sciences, Osnabrück, Germany
[c] Institute of Mechanics and Control Engineering-Mechatronics, University of Siegen, 57068 Siegen, Germany

ARTICLE INFO

Article history:
Available online 4 July 2013

Keywords:
Fatigue crack growth
Duplex stainless steel
475° Embrittlement
Constitutive modeling

ABSTRACT

In order to evaluate the effects that the "475° embrittlement" produces on the fatigue life during high-cycle fatigue, stress-controlled cyclic loading tests were conducted on a standard duplex stainless steel in two different heat treatment conditions (homogenized and embrittled). Transmission (TEM) and scanning electron microscopy (SEM) in combination with automated electron back-scattered diffraction (EBSD) techniques were carried out to analyze the surface damage as well as the initiation and propagation of fatigue cracks. These studies have revealed that the fatigue limit of the embrittled samples is substantially larger than that of the conventional samples at 10^7 cycles in the homogenized condition. Finally, an existing numerical short-crack propagation model was adapted using the stereological values obtained by EBSD to reproduce the propagation of microstructural fatigue cracks in the homogenized and embrittled conditions.

© 2013 Elsevier Ltd. All rights reserved.

1. Introduction

Duplex stainless steels (DSS) are commercially attractive because of the excellent combination of mechanical properties and corrosion resistance obtained from a balanced amount of ferrite and austenite in the microstructure. However, this grade of steel embrittles when exposed in the temperature range of 280–500 °C limiting its application to temperatures below 280 °C. This phenomenon is called "475 °C embrittlement" since the rate of embrittlement is the highest at 475 °C. The main drawback of this embrittlement is that it modifies the tensile and fracture behavior of this steel. Many applications imply cyclic loading and thus the prediction of the fatigue life as well as the knowledge of fatigue limit is essential. Fatigue limit is based on the assumption that below a certain stress value no cycle-dependent damage occurs. Krupp et al. [1] have found that a standard DSS exhibits a technical fatigue limit up to $N = 10^8$ cycles since phase boundaries were identified as effective barriers against slip transfer. In the embrittled material, the information about cyclic behavior is very scarce. Recently, it was reported that fatigue life of a standard DSS at lower strain amplitudes is longer in the aged condition as compared to the non-aged condition. It becomes similar at intermediate strain amplitudes and it is shorter at higher strain amplitudes [2]. Crack initiation and growth in individual grains in DSS depend on the orientation, inherent strength and toughness properties of neighboring grains and it is very important to know and understand how these factors determine fatigue damage evolution. The aim of this work is to evaluate the effect that the "475° embrittlement" could produce on the fatigue life during HCF. Damage evolution and crack propagation studies were carried out combining scanning electron microscopy observations (SEM) with electron backscattered diffraction (EBSD) measurements. Moreover, the dislocation structure was analyzed and correlated with the formation and propagation of microcracks.

* Corresponding author at: Instituto de Física Rosario – CONICET, Universidad Nacional de Rosario, Argentina. Tel.: +54 3414808545.
E-mail addresses: marinelli@ifir-conicet.gov.ar, m.marinelli@hs-osnabrueck.de (M.C. Marinelli).

0013-7944/$ - see front matter © 2013 Elsevier Ltd. All rights reserved.
http://dx.doi.org/10.1016/j.engfracmech.2013.03.034

Nomenclature

DSS	Duplex Stainless Steel
HV	Vickers Hardness
HCF	High-Cycle Fatigue
α phase	ferrite phase
γ phase	austenite phase
$\Delta\sigma/2$	stress amplitude
R	stress ratio, $R = \sigma_{min}/\sigma_{max}$
f	frequency
EBSD	Electron Back-Scattered Diffraction
SEM	Scanning Electron Microscope
TEM	Transmission Electron Microscope
SF	Schmid Factor
σ^i_{nn}	stress normal to slip band (element i)
τ^i_{tn}	shear stress parallel to slip band (element i)
b_n	normal displacement
G_{ij}	influence function
$\sigma^{i\infty}_{nn}$	external normal stress
$\tau^{i\infty}_{tn}$	external shear stress
τ_b	resistance to dislocation motion
τ_{crit}	critical shear stress
k_c	cyclic Hall–Petch constant
r	distance between the center of the sensor element and the boundary
ΔCTSD	Crack Tip Slide Displacement
ΔCTOD	Crack Tip Opening Displacement
da/dN	crack propagation rate
α	twist angle of the crack-plane deflection at a grain boundary
β	tilt angle of the crack-plane deflection at a grain boundary
LEFM	Linear Elastic Fracture Mechanics

Finally, a numerical short-crack model, which takes into account the real two-phase microstructure and its elastic/plastic anisotropy, was adapted to the embrittled condition. This model, validated by experimental data, permits to describe quantitatively the propagation behavior of microstructurally short fatigue cracks.

2. Experimental procedure

The present study was carried out on the DSS of German standard 1.4462 with chemical composition: C: 0.02; Cr: 21.9; Ni: 5.6; Mo: 3.1; Mn: 1.8; N: 0.19; P: 0.023; S: 0.002; Fe balance. The effect of the embrittlement on the damage evolution, initiation and propagation of microcracks was evaluated during HCF under stress-controlled cyclic tests in this steel in two different heat treatment conditions, homogenized and 475 °C-embrittled. In order to increase the grain size, the as-received steels was homogenized 4 h at 1250 °C followed by slow-cooling to 1050 °C and water-quenched. The resulting microstructure consists of approximately 50% austenite with a mean grain size of 30 μm embedded in 50% ferrite with a mean grain size of 27 μm, Fig. 1. Finally, the material was aged at 475 °C for 100 h, resulting in an increase of Vickers hardness values in the ferrite from 259 HV in the annealed DSS to 465 HV in the embrittled DSS.

Cylindrical specimens were manufactured for push–pull and rotating bending fatigue tests. The evolution of the fatigue damage was studied on a shallow notch by direct observation in real time using a long-distance QUESTAR optical microscope coupled to a digital camera.

Push–pull fatigue tests were carried out at room temperature in a servo-hydraulic testing system under stress control, $\Delta\sigma/2 = 350$ MPa, stress ratio $R = -1$ and frequency $f = 5$ Hz. The specimens were analyzed by means of analytical SEM (Zeiss Auriga) in combination with automated EBSD and transmission electron microscopy (Philips EM 300, 100 kV).

3. Experimental results and modeling

Rotating bending fatigue tests were carried out to study the effect of the embrittling heat treatment on the fatigue limit of 1.4462 DSS. The results, as shown in Fig. 2, have revealed that the embrittled condition increases the fatigue life compared with the homogenized condition during HCF.

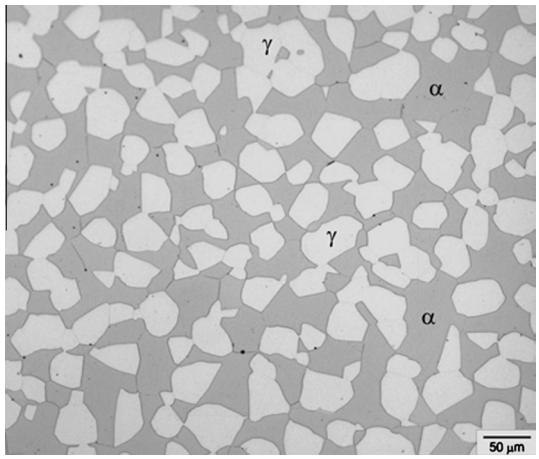

Fig. 1. Optical micrograph on the two-phase structure of 1.4462 DSS after the homogenization heat treatment.

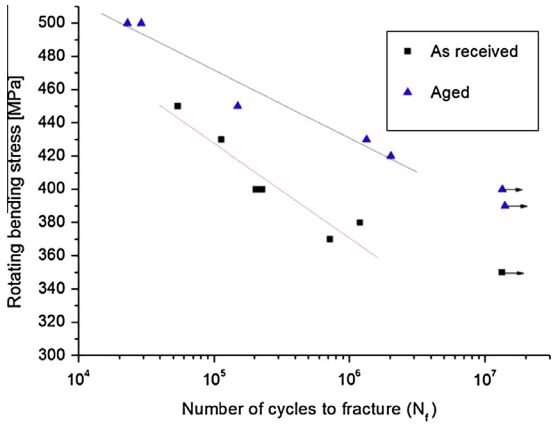

Fig. 2. *S*/*N* (Wöhler) diagram of 1.4462 DSS for rotating bending tests in the homogenized and aged conditions.

When examining the specimen surface during the cyclic tests in the embrittled DSS, the first slip markings appear mostly in the austenitic phase before reaching the first 1000 cycles. As cycling proceeds, slip lines in the austenitic phase intensify and some propagate into the neighboring ferritic grains or remain arrested at boundaries. Therefore, in the embrittled DSS, microcracks often nucleate at α–γ boundaries and then propagate along slip markings formed successively in the austenitic and ferritic grains. As well, microcracks can also nucleate on slip markings in the austenite and at α–α boundary but they are less frequently observed. Fig. 3a shows a microcrack that initiates at the α–γ boundary and propagates on the left-hand crack tip, along the $(1\,\bar{1}\,\bar{2})[1\,\bar{1}\,1]$ system with SF = 0.46 in a ferritic grain, while on the right-hand crack tip, the crack grows in the austenitic grain (black dashed line) by double slip on $(1\,\bar{1}\,\bar{1})[0\,1\,\bar{1}]$ and $(1\,\bar{1}\,1)[1\,1\,0]$ systems with the highest Schmid factor, SF = 0.45 and SF = 0.41, respectively. The corresponding crack length as a function of the number of cycles, for this example of microcrack propagation, is represented in Fig. 3b. According to microcrack growth behavior, phase boundaries represent an efficient barrier to crack propagation. To better understand the microcrack behavior the dislocation structure developed near the surface was analyzed. The characteristic structure developed in some embrittled ferrite grains consists of a cross stitch-dislocation structure as shown in Fig. 4a. However, other grains remain inactive. At the same time, the dislocation structure in the austenite is formed by planar arrangements and dislocation pile-ups, which impinge the phase boundary producing a high stress concentration zone in the neighboring ferritic grain, as shown in Fig. 4b.This important result means that, as cycling proceeds, the increasing pile-ups raise the back stress values producing both a more developed dislocation structure near the phase boundary in the ferritic grain (surrounded by a circle) and a susceptible zone at the phase boundary prone to microcrack nucleation. On the other hand, the fact that the dislocations on the pile-ups are not able to surpass the phase boundary, means that the phase boundaries are rather strong obstacles.

Comparing the results with the homogenized DSS in the same conditions of cycling test, the cyclic plastic activity begins after few cycles in the austenitic phase. As cycling proceeds, slip lines intensify and finally most of them propagate into the ferrite. It is interesting to note that the concentration of stresses in the ferrite increases and slip markings intensify and turn into coarse bands that could remain arrested at the grain boundary. The arrows in Fig. 5a show bands in the ferrite.

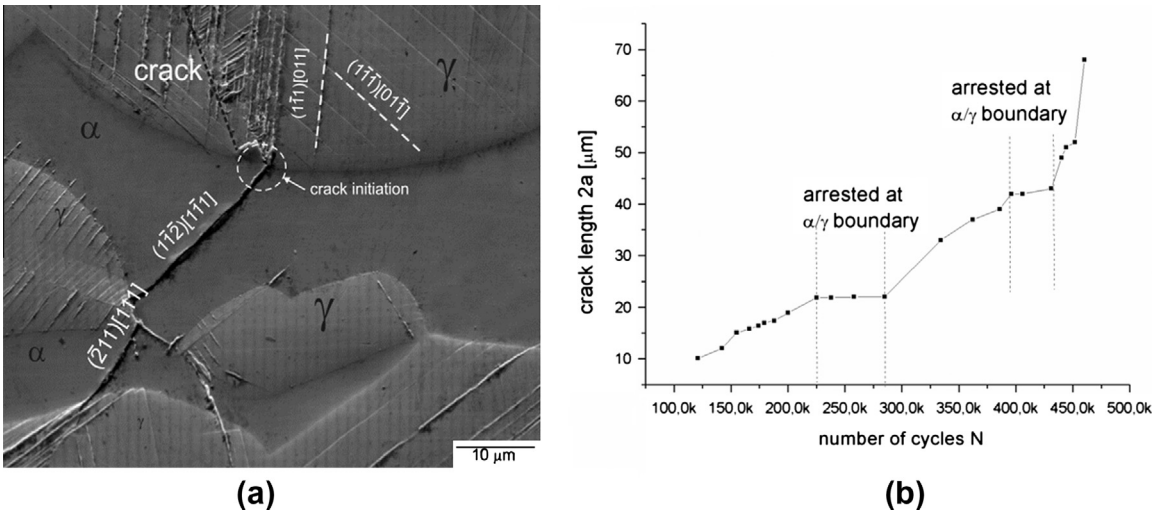

Fig. 3. Aged 1.4462 DSS: (a) scanning electron micrograph showing the crack path after HCF at $\Delta\sigma/2$ 350 MPa and (b) crack length against the number of cycles.

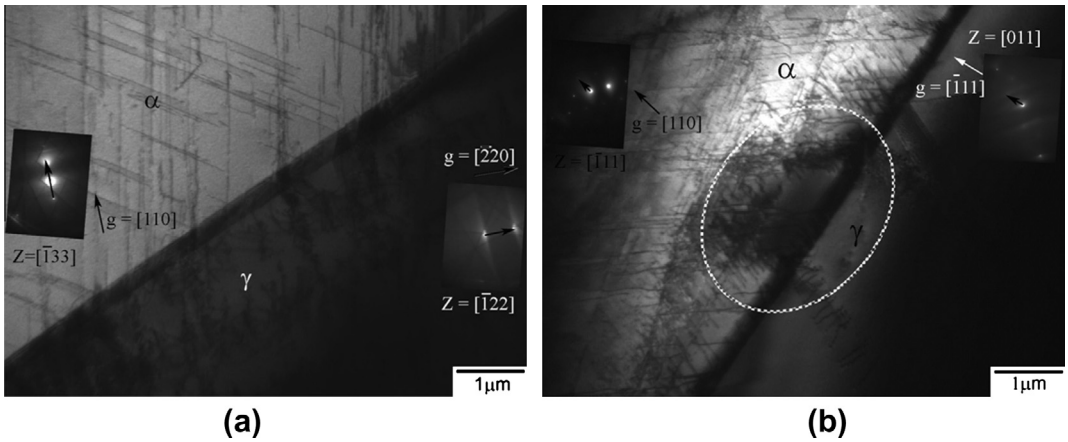

Fig. 4. Aged 1.4462 DSS: (a) cross-stitch dislocation structure in ferrite and (b) high stress concentration zones due to pile-ups of dislocations at grain boundary.

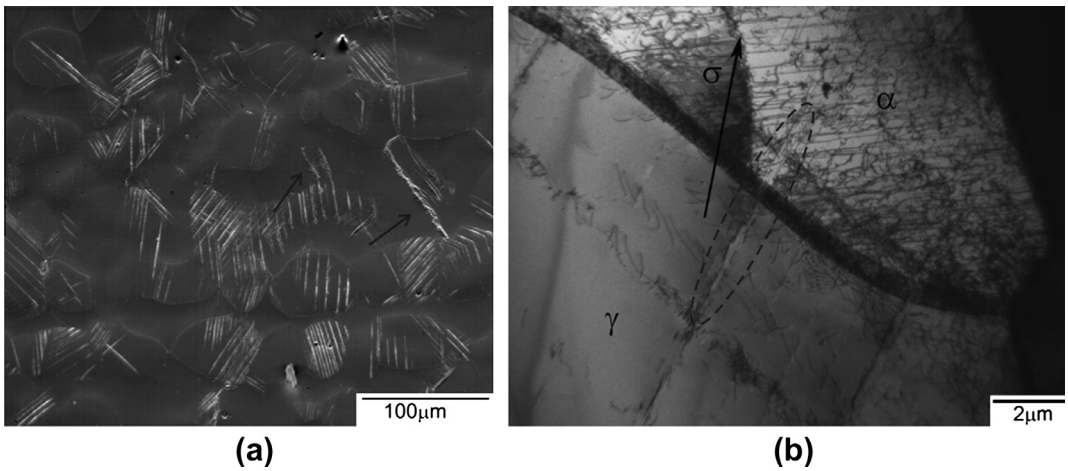

Fig. 5. Homogenized 1.4462 DSS: (a) cyclic plastic activity during HCF and (b) dislocation pile-ups crossing a phase boundary.

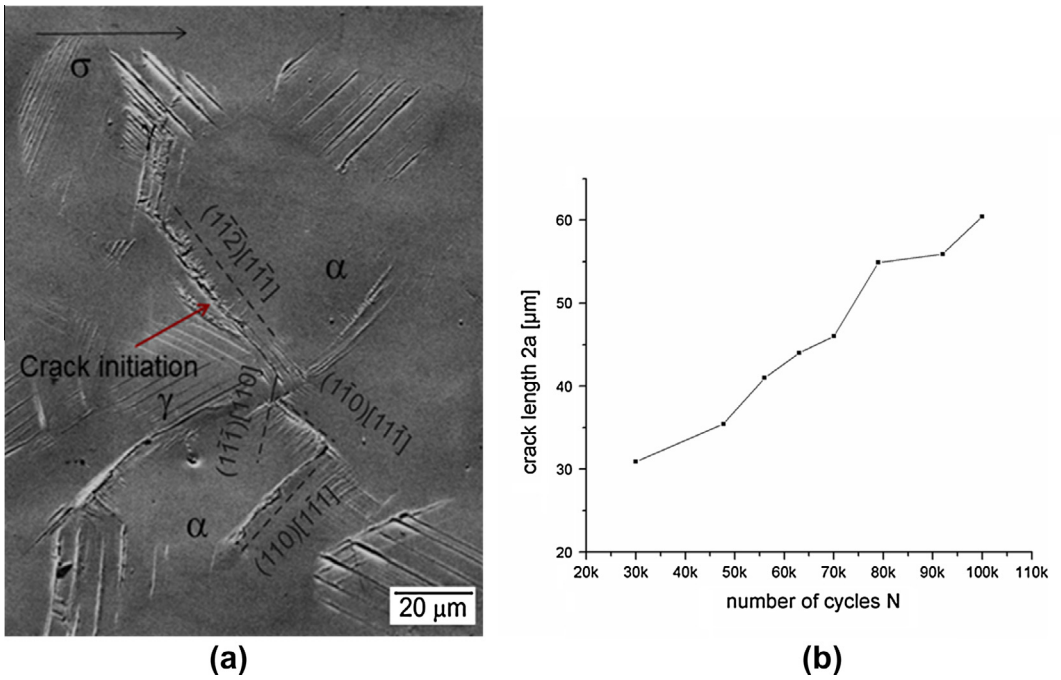

Fig. 6. Homogenized 1.4462 DSS: (a) scanning electron micrograph showing the crack path after HCF at $\Delta\sigma/2$ 350 MPa and (b) crack length against the number of cycles.

As revealed by TEM observations, in the homogenized condition, plastic deformation occurs in both phases. The microstructure in the austenite consists of planar arrangements and dislocation pile-ups in two slip systems while the dislocation structure in the ferrite consists of loop patches of dislocations (Fig. 5b). Particularly, Fig. 5b shows a dislocation band in the austenite that is propagated in the neighbor ferritic grain. In this case, there is not visible high stress concentration at the grain boundary and the dislocations can cross it easily.

Examining the crack propagation, Fig. 6a shows a crack that is initiated in the ferrite on the $(1\,\bar{1}\,\bar{2})[1\,\bar{1}\,1]$ system with the highest SF = 0.47 and after a few cycles the right crack tip propagates into the austenite grain on the $(1\,\bar{1}\,\bar{1})[1\,1\,0]$ slip system with SF = 0.21; this crack remains arrested in the next phase boundary during few cycles and finally surpass it and grows on the $(1\,\bar{1}\,0)[1\,1\,\bar{1}]$ slip system in ferrite with SF = 0.44. On the other hand, the left crack tip grows up to the GB where it remains arrested. This fact is shown as a plateau in Fig. 6b.

4. Crack propagation model

A numerical short-crack model proposed initially by Schick [3] and extended by Künkler et al. [4], have been validated by the experimental data to identify the behavior of the real crack in the present conditions. In this model, plastic slip ahead of a growing microcrack is blocked by the grain boundary until the stress on a dislocation source in the neighboring grain exceeds a critical value. Then, slip is extended to the next grain and the crack propagation rate increases.

The grain microstructure, geometries and crystallographic orientations are obtained by EBSD. The crack and the slip bands are meshed by boundary elements (Fig. 7). The crack elements (i) consist of two dislocation dipoles with a Burgers vector parallel and normal to the crack to allow for sliding and an opening displacement of the crack flanks, respectively. The slip bands ahead of the crack are restricted to tangential displacements (assuming elastic ideal-plastic material behavior), so the respective elements (j) only consist of a dislocation dipole parallel to the crack. The elements are connected to each other by influence functions G_{ij}, which describe the stress in an element i due to a displacement in an element j, [5]. The total stress σ^i_{nn} and τ^i_{tn} are obtained by a summation over all elements (p crack elements and q elements within the slip bands ahead of the crack tip) plus the external normal and shear stresses $\sigma^{i\infty}_{nn}$ and $\tau^{i\infty}_{tn}$. Summation over all elements leads to a system of equation/inequality (Eq. (1)) with the following boundary conditions: (i) neither tensile normal stresses or shear stresses may occur within the crack area, (ii) the normal displacement b_n in the crack area must always be positive, and (iii) within the plastic zones ahead of the crack tip the shear stress τ must not exceed the resistance τ_b to dislocation motion (assumed as to be equal to the microstructural cyclic yield stresses [6]).

$$b_n \geqslant 0 \quad i = 1 \ldots p \tag{1}$$

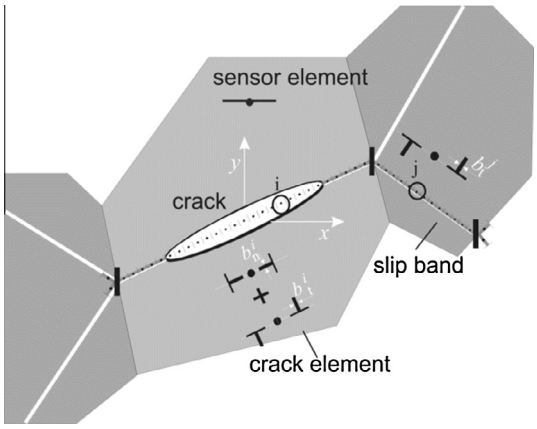

Fig. 7. Model with boundary elements.

$$\sigma^i_{nn} = \sum_{j=1}^{p} G^{ij}_{nn,n} b^j_n + \sum_{j=1}^{p+q} G^{ij}_{nn,t} b^j_t + \sigma^i_{nn,a} \leqslant 0 \quad i = 1 \ldots p$$

$$|\tau^i_{tn}| = \left| \sum_{j=1}^{p} G^{ij}_{tn,n} b^j_n + \sum_{j=1}^{p+q} G^{ij}_{tn,t} b^j_t + \tau^i_{tn} \right| \quad \begin{cases} = 0 & i = 1 \ldots p \\ \leqslant \tau_b & i = p+1 \ldots p+q \end{cases}$$

Therefore, plastic deformation in front of the crack tip occurs, if the shear stress on the slip band exceeds a critical value corresponding to the resistance of dislocations against motion (τ_b). The plastic slip ahead of the growing microcrack is blocked by grain and phase boundaries. To determine the stresses on arbitrary positions around the crack, so-called 'sensor elements' are positioned at the crack tip, which do not represent any displacement. The sensor elements are single boundary elements representing the possible course of the crack path along the slip bands of the adjacent grains or along the grain boundary (intercrystalline crack propagation). Sensor elements in the neighboring grains are added, representing the possible slip systems. When the shear stress caused by the growing crack on one of these sensor elements exceeds a critical value τ_{crit} [7] the corresponding slip band will be meshed in the neighboring grain. Thus, the crack can cross the boundary and propagates along the new slip band until it will be decelerated by the next boundary, resulting in an oscillating crack-growth rate.

Analogous to the model of Navarro and de los Rios [8], the crack propagation rate da/dN (Eq. (2)) is calculated from the range of the crack tip slide displacement ΔCTSD (obtained by a cyclic calculation of the system of inequalities) by means of the power law function, C is a material-specific constant and depends on the stress, m is an exponent (mostly equal to one). The crack tip opening displacement CTOD is zero because the model does not allow normal displacements in the plastic zone. Therefore, crack growth operates only by slide displacement on slip bands parallel to the crack plane. Wilkinson et al. [9] argued that the dislocations of opposite sign are emitted by the crack tip into different parallel slip bands during loading and unloading (slip irreversibility). Hence, the generation of vacancy dipoles causes crack progress.

$$\frac{da}{dN} = C \cdot \Delta\mathrm{CTSD}^m \tag{2}$$

This model takes the crack propagation operating by single and double-slip mechanism into account, i.e., the crack can grow on one slip system resulting in straight crack paths which follow a slip plane with a high Schmid factor or the crack path is the result of two alternating operated slip systems [10]. This model was successfully verified for cracks in homogenized DSS [6]. Consequently, in order to identify the behavior of the real crack in the embrittled DSS, the simulation of crack propagation was applied. The experimentally observed crack was defined in the model using the geometry and crystallographic orientation of the respective grains. The length of the additionally activated slip planes is restricted by the grain boundaries. Moreover, starting cracks were defined according to the experimentally observed ones. Then, these cracks were subjected to cyclic loading calculations. The microstructural cyclic yield stress calculated by Düber et al. [6] for an homogenized DSS was modified for embrittled DSS. As a first approximation the increase in the microstructural cyclic yield stress for the aged ferrite and consequently for the embrittled DSS was considered proportional to the increase in hardness (33% for the aged ferrite and 15% for DSS). Therefore, new data of microstructural cyclic critical yield stress used in the model are: γγ = 137 MPa, αα 262 MPa, duplex = 244 MPa.

The constant C in Eq. (2) was adjusted for the embrittled DSS using the values ΔCTSD obtained by a cyclic calculation of the system of inequalities and da/dN from experimental curve for several cracks, obtaining $C = 0.002$. From these data, Fig. 8 shows the experimental crack and the calculated crack by the proposed model. In the Fig 8b the deceleration in the crack

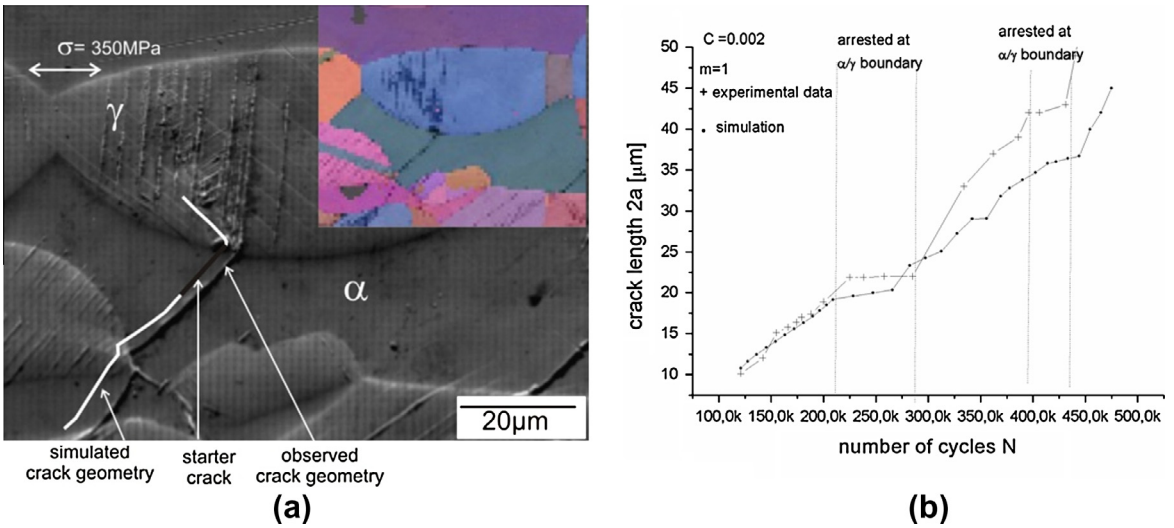

Fig. 8. Aged 1.4462 DSS: (a) scanning electron micrograph showing the crack path and (b) comparison of the calculated and measured values of the crack lengths against the number of cycles during HCF.

propagation rate when the crack approaches boundaries is clearly represented. Therefore, the comparison between experimentally observed and simulated crack demonstrates a good agreement with respect to the crack length as a function of the number of loading cycles.

5. Discussion

In the present study, it was observed that the embrittled condition increases the fatigue life during HCF in comparison with the homogenized condition. It is known that the evolution of surface roughness, subsequent nucleation and growth of short crack in DSS by cyclic loading is strongly influenced by the microstructural parameters, i.e., grain size, grain orientation, grain and phase boundary geometry and precipitates [11]. Consequently, the growth rate of microstructurally short cracks is determined by the crack-tip slide displacement and depends on the resistance against dislocation motion on the slip band ahead of the crack and across microstructural barriers. The main parameters that describe the resistance are the length of the slip band and the local crystallographic misorientation conditions between the slip bands of neighboring grains. According to Zhai et al. [12], the twist (α) and tilt (β) angles of the crack-plane deflection at a grain boundary are the key factors that control the path and growth rate of a short crack. The smaller the twist angle and the tilt angle between two neighboring grains, the lower is the resistance to microcrack propagation. In the present study, the angles α and β were taken into account to analyze both cyclic plastic slip activation and short crack propagation. As regards the coupling between phases in the aged or homogenized DSS, it was observed that when the α and β angles between slip markings in two neighboring austenite and ferrite are less than 10°, the plastic strains of the neighboring grains are compatible, and no stress concentration is developed at the phase boundary, Fig. 9. On the contrary, if α is higher than 10°, the dislocations cannot cross the phase boundary and plastic deformation is accumulated in the first phase – usually the austenite, until a stress concentration occurs at the phase boundary. In a recent study, Taisne et al. [13] observed the role of interfaces in fatigue deformation mechanism in DSS bicrystal and stated that phase boundary geometry and elasticity affect the dislocation transmission process. Moreover, Marinelli et al. [14,15] studied the Kurdjumov–Sachs crystallographic orientation relations between austenite and ferrite in DSS and proposed that the efficiency of the coupling between phases seems to play an important role in the crack formation process.

TEM observations carried out in the homogenized DSS have shown that the deformation is developed in both phases. However, the concentration of stresses in the ferrite increases with cycling and slip markings intensify and turn into coarse bands, which preferably become sites of crack nucleation. Zielinski et al. [16] studied the evolution of dislocation structure in an annealed DSS by in situ TEM straining experiments and reported that the evolution of dislocation structure during straining was dependent on the orientation relationship between the two phases.

On the other hand, in the embrittled DSS some grains of the ferrite are practically inactive and others show low dislocation density such as cross-stitch dislocation structure. However, where the pile-ups in the austenite impinge the phase boundary, the localization of cyclic strain causes the increase of the stress concentration near the phase boundary of the neighboring ferritic grain, creating a more developed dislocation structure as shown in Fig. 4b. As a matter of fact, the high yield stress required to plasticity the embrittled ferrite makes the austenite be the only phase capable to accommodate the deformation. Nevertheless, once the capacity of the austenite grain to plastically deform is reached, the pile-ups generate

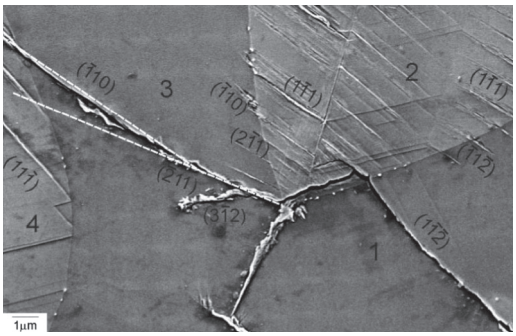

Grains A/B	Slip planes	Angles α, β
1/2	$(\bar{1}1\bar{2})/(1\bar{1}1)$	α=3° β= 7°
2/3	$(1\bar{1}1)/(2\bar{1}1)$ $(1\bar{1}1)/(\bar{2}11)$ $(1\bar{1}1)/(\bar{1}10)$	α=10° β= 0.8° α=66° β= 6° (crack) α=43° β= 10° (crack initiation)
3/4	$(\bar{1}10)/(11\bar{1})$	α=1° β= 2°

Fig. 9. Analysis of the coupling between phases using the Zhai's model in an embrittled 1.4462 DSS.

strong stress concentration zones at the phase boundary capable to allow the nucleation of microcracks and the activation of slip systems in the adjoining ferrite. From the previous results [17,18], it seems that the barrier effect of the phase boundaries is generally higher than the barrier effect of the α–α and γ–γ grain boundaries in the homogenized DSS, irrespective of the angles between possible slip systems in the adjacent grains. Consequently, the aged condition in HCF regime retards plastic deformation in the ferrite and prevents the early crack propagation.

In order to verify the crack propagation model for the embrittled DSS, crack geometries that were observed during fatigue experiments were applied. As an example, Fig. 8 shows a good agreement between experimentally observed and simulated crack propagation. Moreover, the blocking of the slip bands at the grain boundaries as well as the experimentally observed deceleration of the crack growth in the vicinity of the αγ phase boundaries, caused by pile-up of dislocations, could be qualitatively simulated. Some authors [19,20] have reported that the crack propagation rate is strongly influenced by the misorientation of the crack and the slip-direction between grains. Lillbacka et al. [19] have studied the behavior in a duplex steel and they reported that if the slip-directions of a grain were rotated such that the evolution of plastic slip became smaller than for the neighboring grain, the crack propagation rate decreased as the crack approached the grain boundary. According to Krupp et al. [7] the proposed model is able to describe the effect of different kinds of microstructural barriers against crack propagation in a reasonable mechanism-orientated way.

Evaluation of crack paths on the surface of the present embrittled duplex steel revealed that cracks in the austenite phase tend to grow along two alternating slip bands while in the ferrite phase the crack mostly grows on a single-slip plane. Of course, microcrack propagation cannot be attributed only to the effect of ΔCTSD on two-dimensional slip planes. Additionally, three-dimensional crack propagation into the bulk must be taken into account. However, the calculated crack propagation rates for different cracks are in good agreement with the experimental results. Düber et al. [6] argued that the reason for this good agreement is the fact that short crack propagation is governed mainly by the microstructure of the surface grains due to plane stress conditions. In addition, the constant C in the crack propagation law (Eq. (2)) should contain indirectly a factor for the conversion of the two-dimensional model to the three-dimensional crack, analogous to a change in the geometry function when considering three-dimensional cracks instead of two-dimensional cracks in LEFM.

6. Conclusions

In this paper the effect of the embrittlement on the fatigue limit and crack propagation in a duplex stainless steel DIN 1.4462 was studied during high cycle fatigue. It was observed that the embrittled ferritic phase increases the fatigue life in HCF regime, strengthens the phase boundaries and therefore, prevents the early crack propagation. In this regime the plastic deformation is limited to austenite and microcracks initiate mostly at α–γ boundaries and then propagate along slip markings formed successively in the austenitic and ferritic grains. In the homogenized DSS the plastic deformation is present in both phases and the cracks initiate mostly along slip bands in the ferrite.

The two-dimensional model used in this paper allowed to describe quantitatively the propagation behavior of microstructurally short fatigue cracks in an embrittled DSS. The comparison between experimentally observed and simulated cracks demonstrated a good agreement with respect to the crack lengths as a function of number of cycles.

Acknowledgements

This work was supported by the Alexander von Humboldt Foundation, Agencia Nacional para la Promoción de la Ciencia, Técnica and Consejo Nacional de Investigaciones Cientícas y Técnicas (CONICET) and by the cooperation program DAAD/MinCyT between Germany and Argentina.

References

[1] Krupp U, Knobbe H, Christ HJ, Köster P, Fritzen CP. The significance of microstructural barriers during fatigue of a duplex steel in the high- and very-high-cycle-fatigue regime. Int J Fatigue 2010;32(6):914–20.
[2] Sahu JK, Ghosh RN, Christ HJ. Low cycle fatigue behavior of duplex stainless steel: influence of isothermal aging treatment. Fatigue Fract Engng Mater Struct 2009;33:77–86.
[3] Schick A. Ein neues Modell zur mechanismenorientierten Simulation der mikrostrukturbestimmten Kurzrissausbreitung, vol. 18. Düsseldorf: VDI Verlag Reihe; 2004. p. 292.
[4] Künkler B, Düber O, Köster P, Krupp U, Fritzen CP, Christ HJ. Modeling of short crack propagation – transition from stage I to stage II. Engng Fract Mech 2008;75:715–25.
[5] Krupp U. Fatigue crack propagation in metals and alloys. Weinheim: Wiley-VCH; 2007.
[6] Düber O, Künkler B, Krupp U, Christ HJ, Fritzen CP. Experimental characterization and two-dimensional simulation of short-crack propagation in an austenitic–ferritic duplex steel. Int J Fatigue 2006;28:983–92.
[7] Krupp U, Düber O, Christ HJ, Künkler B, Schick A, Fritzen CP. Application of the EBSD technique to describe the initiation and growth behaviour of microstructurally short fatigue cracks in a duplex steel. J Microsc 2004;213:313–20.
[8] Navarro A, de Los Rios ER. Short and long fatigue crack growth: a unified model. Philos Mag A 1988;57:15–36.
[9] Wilkinson AJ, Roberts SG, Hirsch PB. Modelling of the threshold conditions for propagation of stage I fatigue cracks. Acta Mater 1998;46:379–90.
[10] Künkler B, Fritzen CP, Düber O, Krupp U, Christ HJ. Simulation of short crack propagation – transition from Stage I to Stage II. PAMM Proc Appl Math Mech 2005;5:341–2.
[11] Sahu JK, Krupp U, Ghosh RN, Christ HJ. Effect of 475 °C embrittlement on the mechanical properties of duplex stainless steel. Mater Sci Engng A 2009;508:1–14.
[12] Zhai T, Wilkinson AJ, Martin JW. A crystallographic mechanism for fatigue crack propagation though grain boundaries. Acta Mater 2000;48:4917–27.
[13] Taisne A, Decamps B, Priester L. Role of interfaces in duplex stainless steel deformation micromechanisms. Compos Interfaces 2006;13(1):89–102.
[14] Marinelli MC, El Bartali A, Signorelli JW, Evrard P, Aubin V, Alvarez-Armas I, et al. Activated slip systems and microcrack path in LCF of a duplex stainless steel. Mater Sci Engng A 2009;509:81–8.
[15] Marinelli MC, Moscato MG, Signorelli JW, El Bartali A, Alvarez-Armas I. K–S relationship identification technique by EBSD. Key Engng. Mater. 2011;465:415–8.
[16] Zielinski W, Witnicki W, Barstch M, Messerschmidt U. Non-uniform distribution of plastic strain in duplex steel during TEM in situ deformation. Mater Chem Phys 2003;81(2–3):476–9.
[17] Krupp U, Giertler A, Marinelli MC, Knobbe H, Christ HJ, Köster P, et al. Efficiency of grain and phase boundaries as microstructural barriers during HCF and VHCF loading of austenitic–ferritic duplex steel. In: Berger C, Christ HJ, editors. Fifth international conference on very high cycle fatigue. Berlin: DVM; 2011. p. 127–32.
[18] Alvarez-Armas I, Krupp U, Balbi M, Hereñú S, Marinelli MC, Knobbe H. Growth of short cracks during low and high cycle fatigue in a duplex stainless steel. Int J Fatigue 2012;41:95–100.
[19] Lillbacka R, Johnson E, Ekh M. A model for short crack propagation in polycrystalline materials. Engng Fract Mech 2006;73:223–32.
[20] Potirniche GP, Daniewicz SR. Finite element modeling of microstructurally small cracks using single crystal plasticity. Int J Fatigue 2003;25:877–84.